

M3D-K Simulations of Sawteeth and Energetic Particle Transport in Tokamak Plasmas

Wei Shen¹, G. Y. Fu², Zheng-Mao Sheng¹, J.A. Breslau², and Feng Wang³

June 5, 2014

¹Institute for Fusion Theory and Simulation, Zhejiang University, Hangzhou, Zhejiang 310027, China

²Princeton Plasma Physics Laboratory, Princeton, NJ 08543, USA

³School of Physics and Optoelectronic Engineering, Dalian University of Technology, Dalian 116024, China

Abstract

Nonlinear simulations of sawteeth and energetic particle transport are carried out using the kinetic/MHD hybrid code M3D-K. MHD simulations show repeated sawtooth cycles for a model tokamak equilibrium. Furthermore, test particle simulations are carried out to study the energetic particle transport due to a sawtooth crash. The results show that energetic particles are redistributed radially in the plasma core depending on pitch angle and energy. For trapped particles, the redistribution occurs for particle energy below a critical value in agreement with existing theories. For co-passing particles, the redistribution is strong with little dependence on particle energy. In contrast, the redistribution level of counter-passing particles decreases as particle energy becomes large.

1 INTRODUCTION

Sawtooth oscillations, first observed in the 1970s[1], are periodic internal magnetic reconnection events which occur in near axis region in tokamak plasmas. They are mainly caused by internal kink mode with helicity $m/n = 1$, and are characterized by repeatedly collapse of the central plasma temperature. Sawtooth oscillations can induce significant transport of energetic particles (beam ions, bulk particles energized by auxiliary heating, and fusion products). In burning plasmas such as in ITER[2] sawteeth can increase alpha particle losses and damage the first wall of fusion reactors. So far, the sawteeth-induced redistribution of energetic particles has been observed and studied in many experiments[3, 4, 5, 6, 7, 8].

Initial theoretical studies[9, 10] of energetic particle transport due to sawtooth oscillations simply treated energetic particles as bulk plasmas and assumed that the particles are attached to magnetic flux surfaces. Later, the importance of toroidal precession drift was demonstrated and a critical energy was found[11, 12, 13], above which the frozen-in-line condition is broken and the trapped particles are slightly redistributed. This prediction was confirmed in recent experiments on DIII-D[6]. Finally, resonance between energetic particles and the electromagnetic fields of the sawteeth was considered[14, 15]. These results have been reviewed in [16]. Also, the effect of high β (the ratio of bulk plasma pressure to the magnetic field pressure) was studied in spherical tori and was found to play an important role on trapped particles[17].

Two approaches have been used to describe the background sawtooth, which are used to simulate energetic particle transport. The first approach assumes full magnetic reconnection and applies theoretic models to describe background sawteeth, and the second approach prescribes electromagnetic perturbation based on experimental measurements. Kolesnichenko et al.[11, 12] simulated energetic particle transport due to a sawtooth which evolved based on Kadomtsev model[18]. Zhao and White[19] modeled sawtooth mode structure and evolution based on experimental parameters and simulated alpha particle transport in TFTR. They found that the stochasticity of magnetic field lines was important for alpha particle redistribution. Farengo et al.[20, 21] reconstructed the mode structure and temporal variation of sawteeth from the experimental data. However there has been little work so far on using self-consistently evolving background sawteeth to study energetic particle transport.

In this work, the background sawteeth are self-consistently studied by using the resistive MHD model with M3D-K code and the corresponding energetic particle transport is simulated using test particle approach. Our simulation results show that energetic particles are redistributed radially in central plasma region and the redistribution level depends strongly on pitch angle and energy. For the trapped particles, there exists a critical energy above which particles are weakly redistributed. This result is consistent with existing theories. For the passing particles, the co-passing particles are strongly redistributed, and the redistribution of the counter-passing particles becomes weaker as the particle energy increases. The mechanism for the difference in the behaviors between the co-passing and counter-passing particles is investigated.

This article is organized as follows: Sec. II briefly introduces the code and parameters used in our simulation; Sec. III describes and analyses the simulation results of sawteeth and related energetic particle transport; Discussion and summary are given in Sec. IV.

2 M3D-K MODEL AND BASIC PARAMETERS

2.1 Numerical models used in M3D-K

The 3D nonlinear extended MHD code M3D-K is used in our simulation, and the kinetic/MHD hybrid model is applied in M3D-K which treats thermal ions and electrons as a single fluid and describes energetic particles using

drift kinetic equation. For the MHD part, the dissipative MHD model consists of the full resistive MHD equations and additional dissipative terms including viscosity and heat conduction as well as sources of particle, momentum, and heat[22]. In addition, the artificial sound wave method is used to model fast thermal conduction along magnetic field lines(Eq. (8) and (9) in the Ref. [22]). For the energetic particle part, Particle-In-Cell(PIC) method is employed[24]. The M3D-K code has been widely applied to study MHD modes and energetic particle instabilities in tokamaks[23, 24, 25, 26, 27, 28, 29].

2.2 Parameters and initial profiles

In this work, a circular cross-section tokamak with aspect ratio $R_0/a = 4$ is simulated, and Spitzer resistivity profile is $\eta(T) = \eta_0(T/T_0)^{-3/2}$, where η_0 and T_0 are the resistivity and temperature at the magnetic axis. In our simulation, $\eta_0 = 10^{-5}$ and correspondingly Lundquist number $S = 1/\eta_0 = 10^5$. The initial equilibrium is obtained from the equilibrium code VMEC. The pressure profile is given by $p(\Psi) = p_0[0.75(1 - \Psi) + 0.25\exp(-\Psi/0.25)]$, where Ψ is the normalized poloidal flux variable varying from 0 at axis to 1 at the edge of the plasma, central thermal beta $\beta_0 = 4.38\%$, The safety factor profile is given by

$$q(\Psi) = q_0 + \Psi[q_1 - q_0 + (q'_1 - q_1 + q_0)\frac{(1 - \Psi_s)(\Psi - 1)}{\Psi - \Psi_s}], \quad (1)$$

where $\Psi_s = (q'_1 - q_1 + q_0)/(q'_0 + q'_1 - 2q_1 + 2q_0)$, $q_0 = 0.7$, $q_1 = 3.6$, $q'_0 = 2.0$, and $q'_1 = 5.0$. Fig. 1 plots the equilibrium pressure and q profiles.

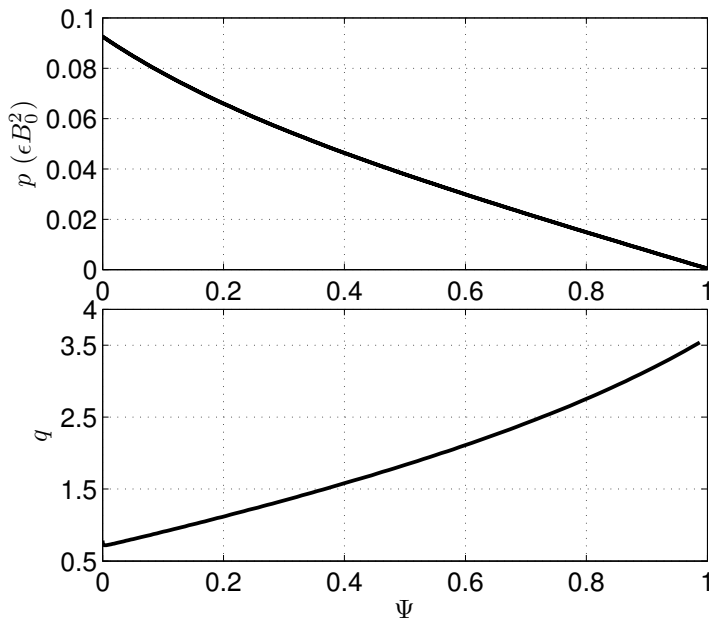


Figure 1: Equilibrium profile of pressure and q.

Energetic particles are loaded with discrete values of pitch angle and energy and are distributed exponentially in radial direction,

$$f = \sum_{i,j} \exp(-\langle \Psi \rangle / 0.25) \delta(E - E_i) \delta(\Lambda - \Lambda_j), \quad (2)$$

where $\Lambda \equiv \mu B_0 / E$ is the pitch angle, and $\langle \Psi \rangle$ is Ψ averaged over the particle orbit. Using the definition of toroidal angular momentum, we obtain

$$\langle \Psi \rangle = p_\phi / e - \frac{M}{e} \left\langle v_\parallel R \frac{B_\phi}{B} \right\rangle, \quad (3)$$

where e and M is the particle charge and mass respectively. We use the following approximations for simplicity[24],

$$\left\langle v_\parallel R \frac{B_\phi}{B} \right\rangle \approx 0 \quad (4)$$

for trapped particles and

$$\left\langle v_\parallel R \frac{B_\phi}{B} \right\rangle \approx \text{sign}(v_\parallel) v R_0 \sqrt{1 - \mu B_0 / E} \quad (5)$$

for passing particles, where B_0 and R_0 is the magnetic field amplitude and major radius at the magnetic axis respectively.

3 SIMULATION RESULTS AND ANALYSIS

3.1 Numerical Results

3.1.1 Background sawteeth results with M3D code

In this section we present the MHD simulation results using M3D code. The linear simulation of the given equilibrium finds an unstable kink mode with dominant mode number $n = m = 1$. The mode structure is shown in FIG. 2. We observe that the mode is mainly located inside the $q = 1$ rational surface. The calculated linear growth rate is $\gamma \tau_A = 0.0283$, where τ_A is the Alfvén time: $\tau_A \equiv R_0 / V_A$. Furthermore, the mode is ideally unstable with $\gamma \tau_A = 0.544\%$ at $\eta = 0$. As shown in FIG. 3, for S ranging from 3.33×10^4 to 10^6 , the linear growth rate scales as $S^{-1/3}$. According to Ref. [30] the mode is a resistive internal kink although this mode is ideally unstable.

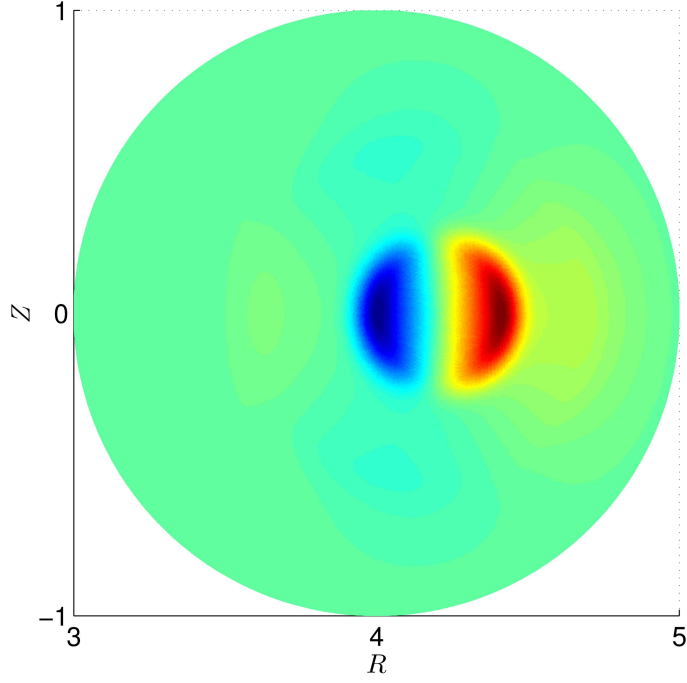


Figure 2: Velocity stream function U of the eigenmode.

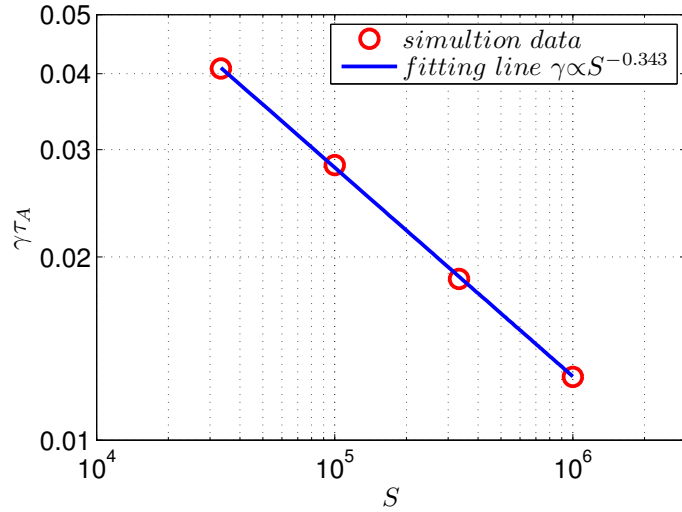


Figure 3: The linear growth rate versus Lundquist number S . $S = 3.33 \times 10^4, 10^5, 3.33 \times 10^5, 10^6$ respectively.

Now we turn to the nonlinear study with M3D code. To initialize the nonlinear simulation, the current and heat sources are prescribed to maintain the equilibrium current and pressure profiles steady state without 3D perturbation. The 3D nonlinear simulation starts with an $n = 1$ perturbation which evolves into an $n = 1, m = 1$ internal kink

instability. FIG. 4(a) shows the evolution of the total kinetic energy and the central temperature $T(0)$. Here time is normalized as the Alfvén time τ_A . We observe that periodic sawtooth oscillations are successfully simulated. It should be noted that the first sawtooth crash has a much larger kinetic energy as compared to those of subsequent crashes because it depends on details of the initial conditions. Therefore we determine the sawtooth period from the subsequent repeated sawtooth crashed. This gives the sawtooth period around $328\tau_A$. As shown in FIG. 4(b), toroidal modes up to $n=6$ are kept in our simulation, different mode are coupled together with the $n = 1$ mode being the dominant one.

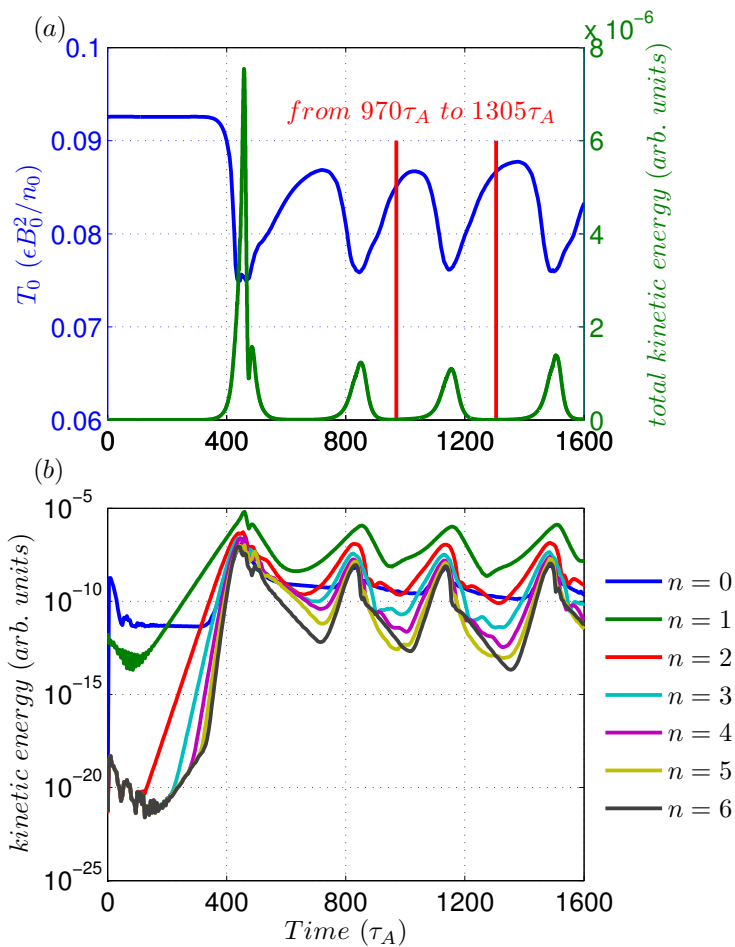


Figure 4: (a) Evolution of total kinetic energy and $T(0)$. In the next section energetic particle transport is simulated from $t = 970\tau_A$ to $t = 1305\tau_A$. (b) Evolution of kinetic energy of different toroidal number n .

Our results show that the resistive internal kink mode results in complete magnetic reconnection in a sawtooth crash similar to the Kadomtsev model[18]. Time evolution of the magnetic flux surfaces during one typical sawtooth cycle is shown in FIG. 5. First, a magnetic island forms around the $q = 1$ rational surface. Then, during the growth of the magnetic island, the sawtooth crash mixes the central plasma region with the outer region, resulting in cooling

of the core. As the current source drives the safety factor q below unity in the central region and the pressure source heats up the cooled core region, the magnetic surfaces are almost recovered in the core region and the magnetic island becomes the new axis. Then the sawteeth cycle repeats again.

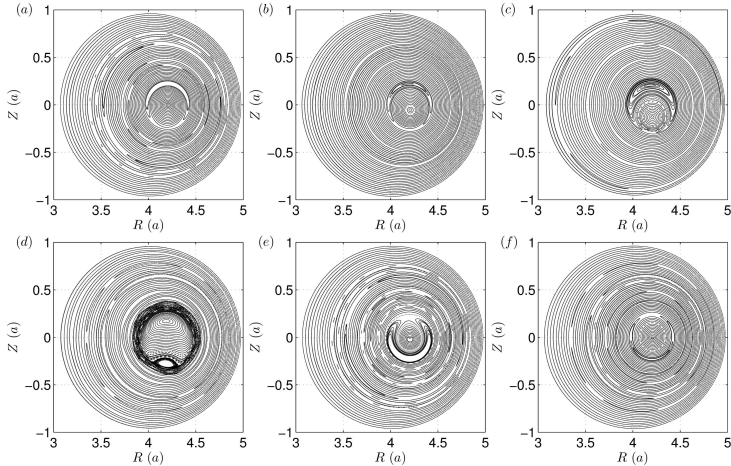


Figure 5: Poincaré plots of magnetic surfaces at $\phi = \pi/2$ shows the evolution of sawteeth during one period. (a) Initial state: $t = 970\tau_A$. (b) Before second crash: $t = 1030\tau_A$. (c) Island growing: $t = 1100\tau_A$. (d) After second crash: $t = 1145\tau_A$. (e) Nonlinear phase: $t = 1220\tau_A$. (f) Final state: $t = 1305\tau_A$. (a) and (f) corresponds to mostly recovered flux surfaces.

3.1.2 Energetic particle transport using M3D-K code

We now present the results of energetic particle transport due to a sawtooth. The background sawteeth is self-consistently simulated using the resistive MHD model as shown above. The magnetic surfaces at $t = 970\tau_A$ and $t = 1305\tau_A$ are mostly recovered (as shown in FIG. 5(a) and FIG. 5(f)), so the energetic particle redistribution is simulated within this time period and the crash time of the sawtooth cycle is around $115\tau_A$ (from $t = 1030\tau_A$ to $t = 1145\tau_A$).

Here we briefly interpret the physical picture of energetic particle transport given by Kolesnichenko et al. [11, 12]. The energetic particles are assumed to have small orbit width $\Delta r_b \ll r_{mix}$, where Δr_b is the particle orbit width and r_{mix} is the sawtooth mixing radius. Considering the bounce-averaged motion of a particle, there are three characteristic time scales to determine the property of energetic particles' transport due to a sawtooth: (1) the toroidal precession duration τ_{pr} which is related to the particle toroidal drift motion, (2) the longitudinal time τ_ψ which represents for the characteristic time of the bounce-averaged motion along the helical perturbed flux surfaces, (3) the crash time τ_{cr} which is the duration of the $E \times B$ drift motion. If the sawtooth crash is sufficiently fast ($\tau_{cr} \ll \tau_{pr}$), energetic particles are attached to magnetic field lines and move together with the evolving flux surfaces due to the $E \times B$ drift, but the redistribution is weakened by the toroidal precession drift as the particle toroidal precession

motion leads to strong phase mixing and decorrelation between the particle motion and the sawtooth, whereas the effect of the toroidal precession motion is weakened by the particle longitudinal motion. For the trapped particles $\tau_\Psi = \tau_{pr}/|q-1|$, and for the passing particles $\tau_\Psi = \tau_t/|q-1|$, where τ_t is the particle transit time. As in our simulation, during one sawtooth period, q is almost unity inside the sawtooth range, so we just need to compare τ_{pr} with τ_{cr} and the condition for weak redistribution is: $\tau_{pr} \ll \tau_{cr}$.

Also the third adiabatic invariant could be applied to get the condition above. when $\tau_{pr} \ll \tau_{cr}$, the third adiabatic invariant $J_3 = \int v_d dl$ is almost unchanged, as a result particles are weakly redistributed. $\tau_{pr} = \tau_{cr}$ gives the critical energy of trapped particles,

$$E_{crit} = 2\pi M k_s r_s R_0 \omega_B / \tau_{cr}, \quad (6)$$

where M is the ion mass, k is the ellipticity, ω_B is the cyclotron frequency and the subscript 's' means the values at the $q=1$ flux surface.

Energetic particles are loaded as given in Eq. (2), and the redistribution level of different type of energetic particles is shown in FIG. 6, and the redistribution level is defined as

$$\int |\delta f| dP_\phi / \int f dP_\phi \equiv \frac{\int |f(t) - f(t = 970\tau_A)| dP_\phi}{\int f(t = 970\tau_A) dP_\phi}, \quad (7)$$

here $P_\phi = p_\phi/e$ represents the particle radial position, and energy is normalized by E_{crit} which is calculated according to Eq. (6). E_{crit} corresponds to

$$v_h/v_A = 0.7275, \quad \rho_h/a = 0.04656, \quad (8)$$

where v_h and ρ_h are the velocity and gyroradius of the particles with energy equals E_{crit} .

From FIG. 6 the results show that energetic particles are redistributed depending on pitch angle and energy. For the trapped particles and counter-passing particles, the redistribution level decreases as the particle energy becomes large. For the co-passing particles, the redistribution is strong with little dependence on the particle energy. Detailed distribution functions of energetic particles with three discrete energy at $t = 970\tau_A$ and $t = 1305\tau_A$ are shown in FIG. 7. In the following ψ denotes for the poloidal flux. As the orbit width is small for the $0.25E_{crit}$ particles, According to Eq. (3), (4) and (5), compared to the initial distribution at $t = 970\tau_A$, the distribution for all types of particles at $t = 1305\tau_A$ is reduced for $\langle\psi\rangle$ is less than -0.247 , and increased with $\langle\psi\rangle \in [-0.247, -0.2]$, and is almost unchanged where $\langle\psi\rangle$ is larger than -0.2 . As the $q = 1$ surface is located at $\psi = -0.247$, and the sawtooth boundary is found to be around $\psi = -0.2$, so energetic particles inside $q = 1$ surface is transported out of the $q = 1$ surface due to magnetic reconnection effect, and the radial range of the redistribution is inside the sawtooth region.

Time evolution of the redistribution level is shown in FIG. 8, from which we can see that after the sawtooth crash ($t = 1145\tau_A$), energetic particles are still transported and the redistribution level becomes saturated around $t = 1220\tau_A$. As shown in FIG. 5(e), at $t = 1220\tau_A$ the new magnetic axis forms and the change of magnetic flux is relatively small from $t = 1220\tau_A$ to $t = 1305\tau_A$. Since the redistribution of energetic particles is as a result of

particles moving with the magnetic flux surfaces, the redistribution level of energetic particles are almost unchanged during this time period.

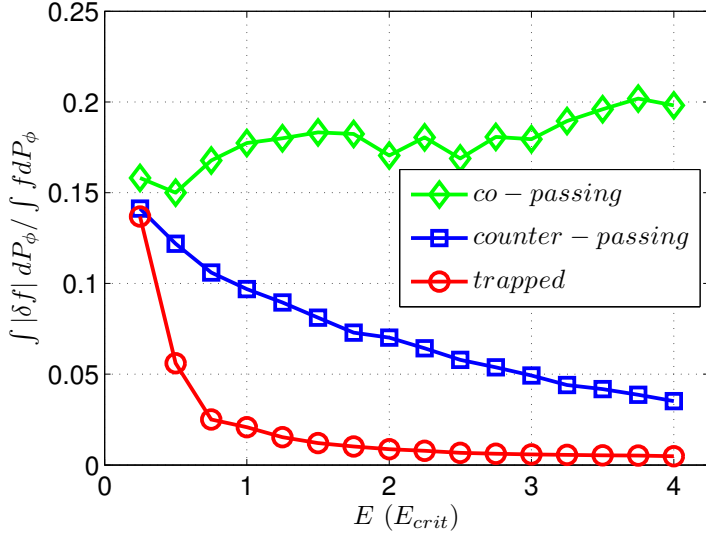


Figure 6: Redistribution level of different type of energetic particles versus energy. Energetic particles are loaded with 16 equidistant energies from $E_{crit}/4$ to E_{crit} . Pitch angle of trapped particles is $\Lambda = 1.0$, and of both co-passing and counter-passing particles is $\Lambda = 0.0$.

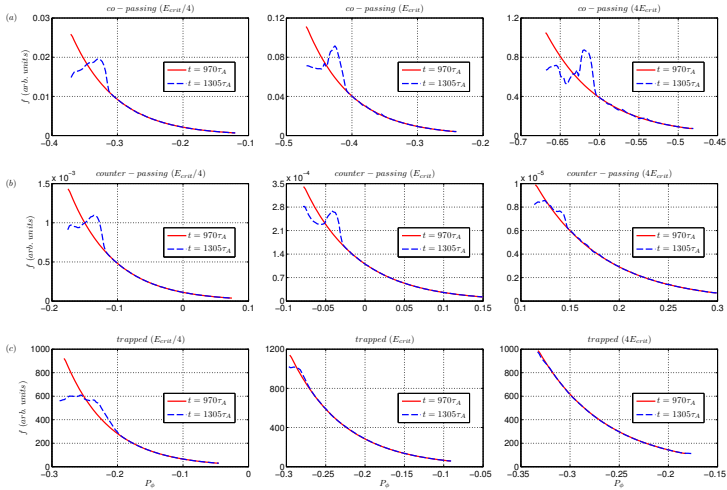


Figure 7: Distribution function of different type of energetic particles with different energy at initial state and final state. (a) Co-passing particles. (b) Counter-passing particles. (c) Trapped particles.

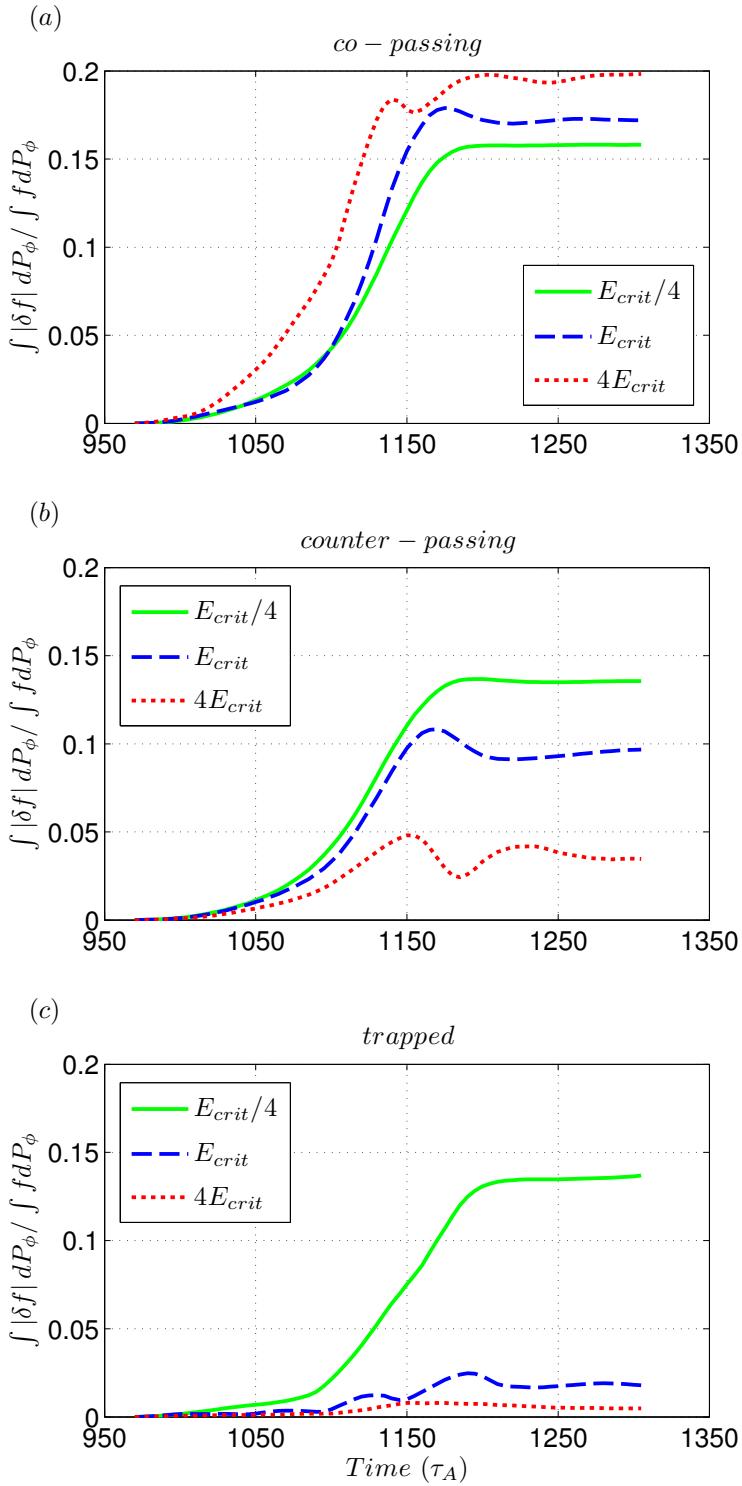


Figure 8: Redistribution level of energetic particles with energy equals $E_{crit}/4$, E_{crit} , $4E_{crit}$ versus time. (a) Co-passing particles; (b) Counter-passing particles; (c) Trapped particles.

3.2 Analysis of results on trapped particles

For trapped particles, as mentioned above, the $q = 1$ surface is located at $\psi = -0.247$. FIG. 9 shows the precession frequency of trapped particles as a function of energy and averaged ψ . Averaged ψ is defined as $(\psi_{max} + \psi_{min})/2$, where ψ_{max} and ψ_{min} is the maximum and minimum of poloidal flux for a particle to go through in one bounce/transit period. When the energy of the trapped particles is larger than $0.8E_{crit}$, the particles inside the $q = 1$ surface have strong toroidal precession drift and they would be weakly redistributed, as the red line shown in FIG. 6.

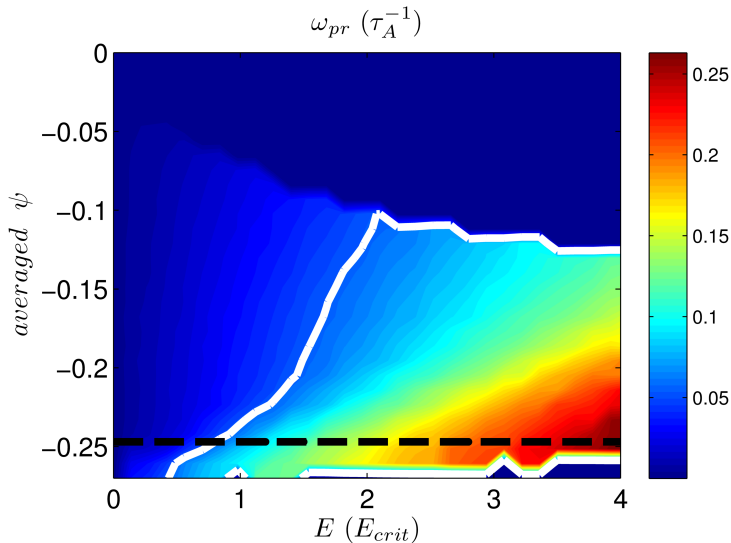


Figure 9: Precession frequency of trapped particles. The dashed line(black) shows $q = 1$ surface location, and the solid line(white) represents for $\omega_{pr} = 2\pi/\tau_{cr}$, and the solid line and the dashed line intersects around $0.8E_{crit}$.

To investigate the scaling of the critical energy, we scan the sawtooth crash time by varying resistivity. The results of the redistribution levels of trapped particles from such a scan are shown in FIG. 10(a), here E_{crit} is normalized by different crash time of the background sawtooth. We denote redistribution level as $g \equiv \int |\delta f| dp_\phi / \int f dp_\phi$, and define the critical energy in our simulation as the first point when $|\partial g / \partial E| < 0.02$, and is labeled as E_{sim} , and relationship between E_{sim} and the crash time is shown in FIG. 10(b). We observe that that the critical energy from our simulations is approximately inversely proportional to the crash time as previously predicted[11] (see Eq. (6)). Also from Eq. (6), the critical energy of trapped particles is independent of the particle mass. This is confirmed by our simulation results as shown in FIG. 11.

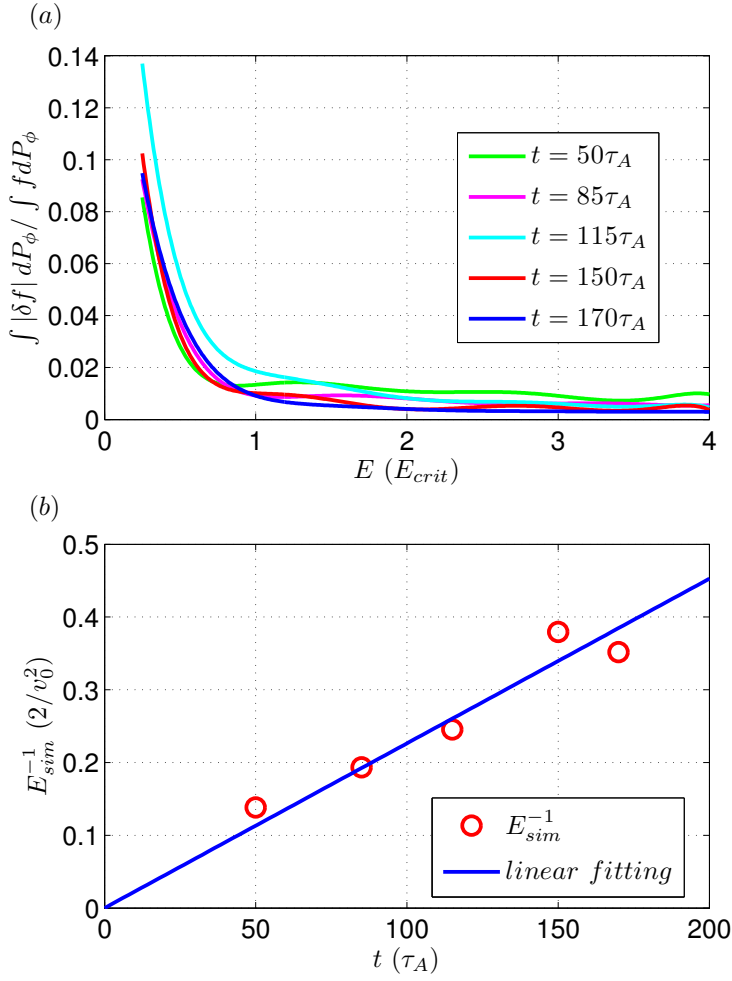


Figure 10: (a) Redistribution level of trapped particles due to sawteeth with different crash times. (b) Reciprocal of E_{sim} as a function of crash time. E_{sim} is normalized by $v_0^2/2$, where $v_0 \equiv \epsilon v_A = a v_A / R_0$.

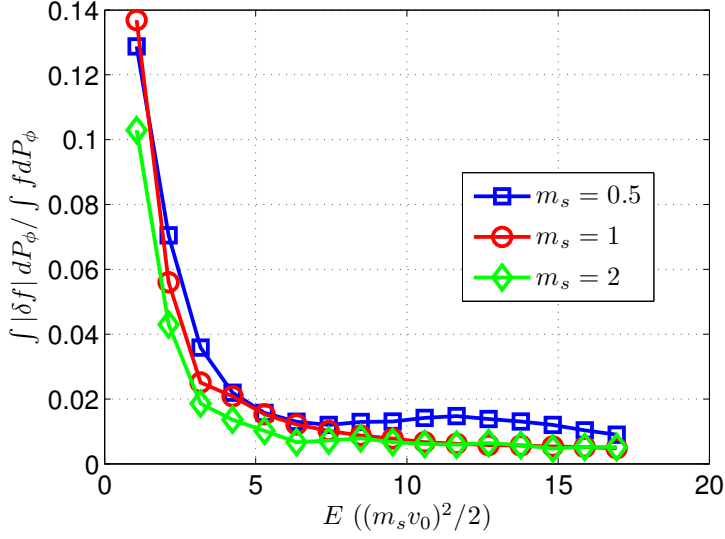


Figure 11: Redistribution level of trapped particles with different mass, m_s is a factor proportional to mass, and $m_s = 1$ corresponds to baseline case.

3.3 Analysis of results on passing particles

When the orbit width Δr_b of passing particles is small ($\Delta r_b \ll r$, where r is the radial coordinate) and the plasma cross section is circular, the precession frequency is given by[31][32]

$$\omega_{pr} = \xi \frac{v^2}{R_0^2 \omega_{B0}} = aE + \sigma_v b m^{1/2} E^{3/2}, \quad (9)$$

where

$$\xi = q \left(\frac{1}{q^2} - 1 - \frac{3\Delta'}{2\epsilon} - \frac{r\Delta''}{2\epsilon} + \sigma_v \frac{\hat{s}q\rho}{r\epsilon} \right), \quad (10)$$

$\omega_{B0} = eB_0/Mc$ with $B_0 = B(r=0)$, $\rho = v/\omega_{B0}$, $\Delta' = d\Delta/dr$, $\Delta'' = d^2\Delta/dr^2$ and $\sigma_v \equiv \text{sign}(v_{\parallel})$. From Eq. (9) we see that the precession frequency of co-passing and counter-passing particles is quite different and the difference becomes larger when particle energy increases.

Comparison of precession frequency of passing particles calculated from Eq. (9) and from our simulations is shown in FIG. 12, they are almost the same within the $q = 1$ surface.

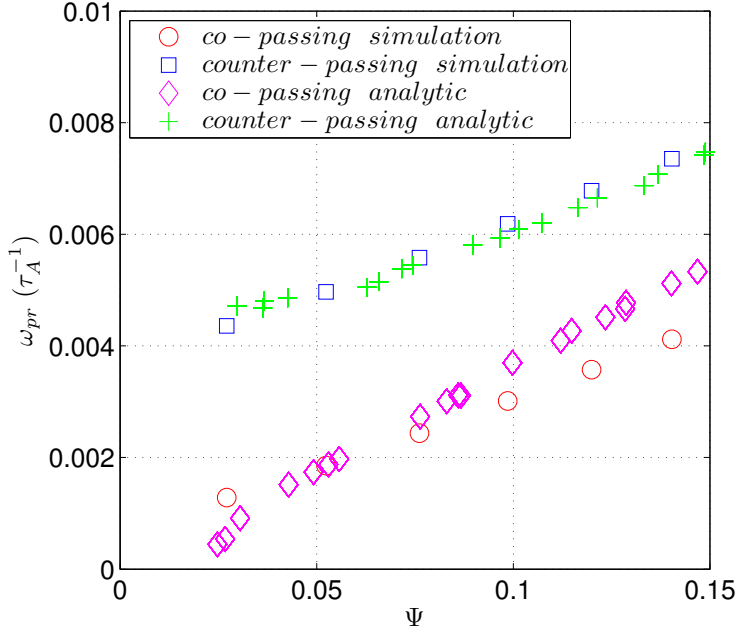


Figure 12: Precession frequency of passing particles as a function of normalized poloidal flux variable Ψ , here 'simulation' denotes for simulation results, and 'analytic' means calculated values from Eq. (9). As shown in FIG. 1, $\Psi = 0.145$ corresponds to $q = 1$ surfaces.

The precession frequency of passing particles inside the $q = 1$ surface is shown in FIG. 13. For the co-passing particles, inside this region $\omega_{pr} < 2\pi/\tau_{cr}$, so the co-passing particles are strongly redistributed. In contrast, the precession frequency of the counter-passing particles are much larger than the co-passing particles, and when the energy of the counter-passing increases, ω_{pr} would exceed $2\pi/\tau_{cr}$, and correspondingly the redistribution level of the counter-passing particles is weakened.

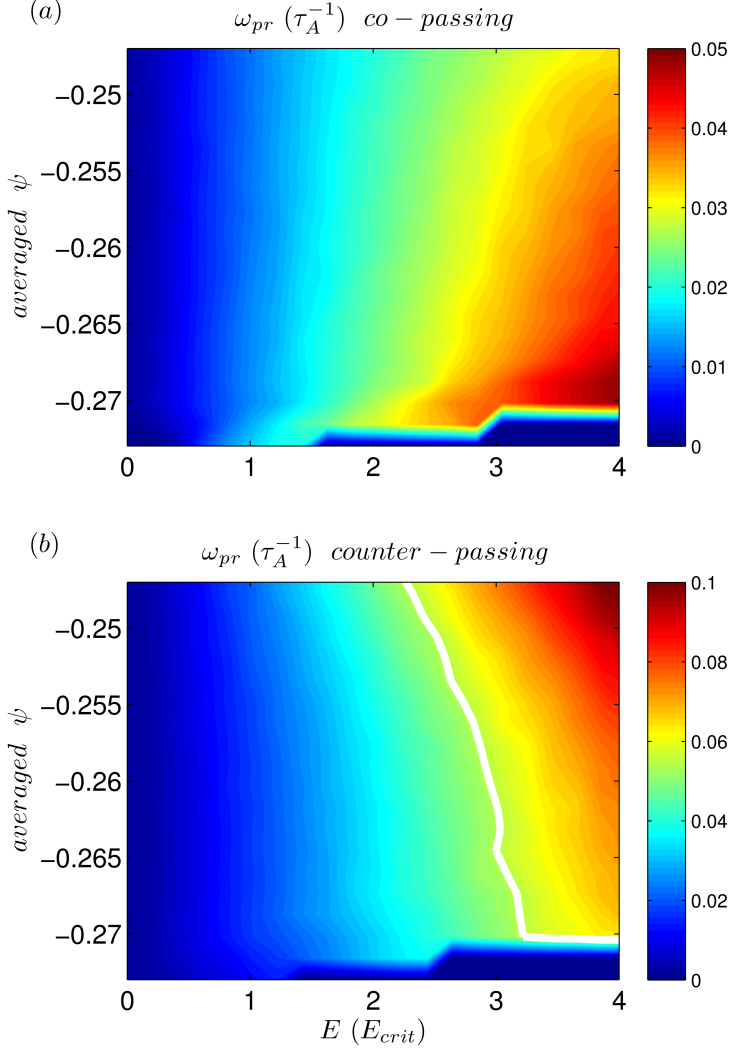


Figure 13: Precession frequency of passing particles. (a) Co-passing particles. (b) Counter-passing particles. In the figure the solid line(white) represents for $\omega_{pr} = 2\pi/\tau_{cr}$.

As shown in FIG. 6, the counter-passing particle redistribution level decreases gradually with energy. For this reason we define E_{sim} of the counter-passing particles roughly as the first point at which the redistribution level is less than 50% of the redistribution level of the counter-passing particles with energy equals $0.25E_{crit}$. From Eq. (9) and the condition $\omega_{pr} = 2\pi/\tau_{cr}$, the critical energy of counter-passing particles would decrease when the sawtooth crash time increases, and this is verified in FIG. 14. Also according to Eq. (9), the critical energy of counter-passing particles would depend on the mass, which is different from that of trapped particles. This is also confirmed in our simulations as shown in FIG. 15.

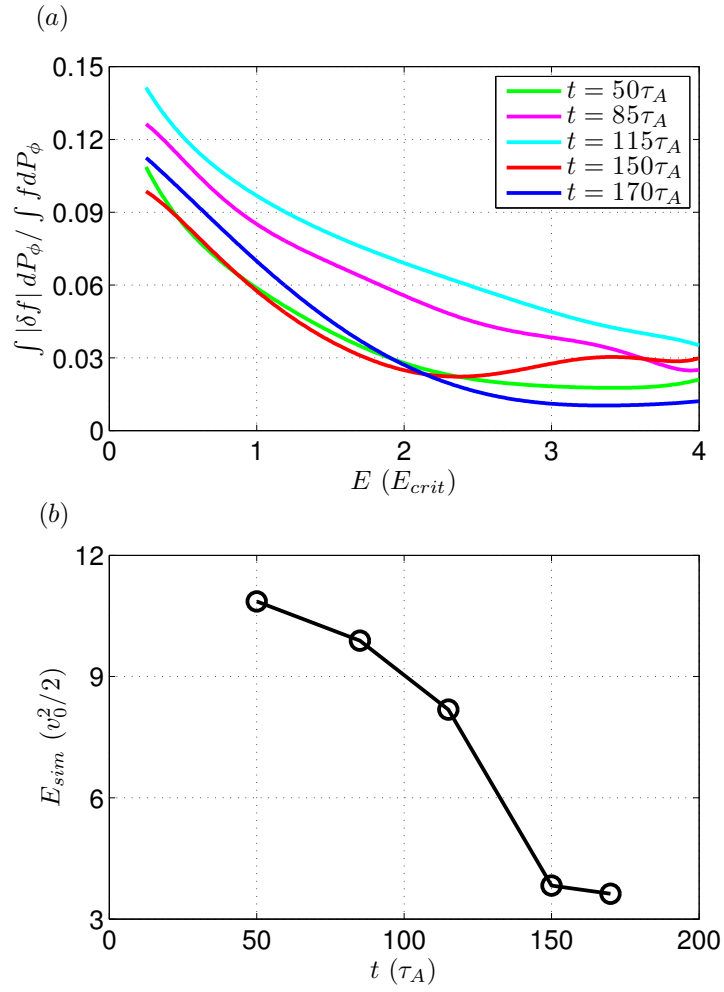


Figure 14: (a) Redistribution level of counter-passing particles due to a sawtooth with different crash time. (b) Critical energy E_{sim} as a function of crash time.

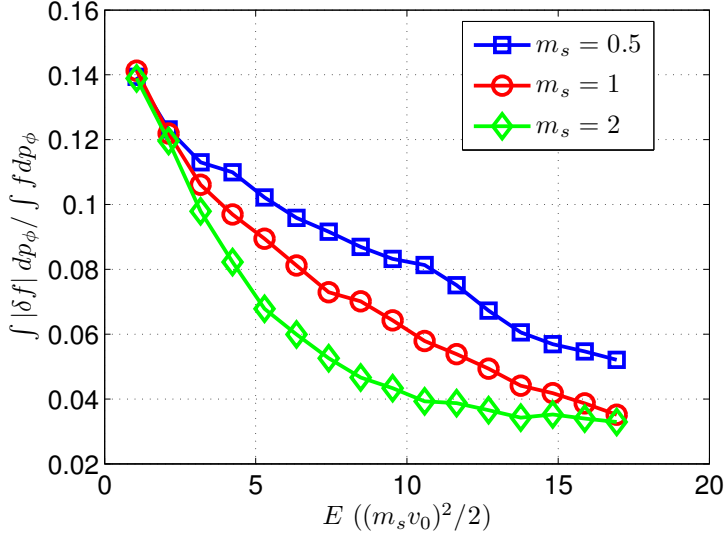


Figure 15: Redistribution level of counter-passing particles with different mass, m_s is a factor proportional to mass, and $m_s = 1$ corresponds to baseline case.

As shown in FIG. 16, the redistribution level of the counter-passing particles with different pitch angle Λ has similar trends as energy increases. When the energy of the co-passing particles is sufficiently large, the redistribution level would decrease either but much slower than the counter-passing particles. Since ρ_h/a is less than 0.1 for present tokamak devices and future tokamak reactors, we focus on the particles with energy less than $4E_{crit}$, and in this energy range the co-passing particles are strongly redistributed.

The difference between the redistribution of co-passing and counter-passing particles is also found recently by Farengo et al.[21]. Actually they found with ITER-like parameters, the co-passing particles are redistributed weaker than the counter-passing particles, and they mentioned that the opposite could happen if the mode is propagating with another direction. In our simulation the mode frequency is almost zero, and if the mode is propagating with finite frequency, the condition $\omega_{pr} = 2\pi/\tau_{cr}$ is changed to $|\omega_{pr} + \omega| = 2\pi/\tau_{cr}$, where ω is the mode frequency. With this condition we could also explain the different redistribution level of passing particles when the direction of mode propagation is changed as the sign of ω is changed.

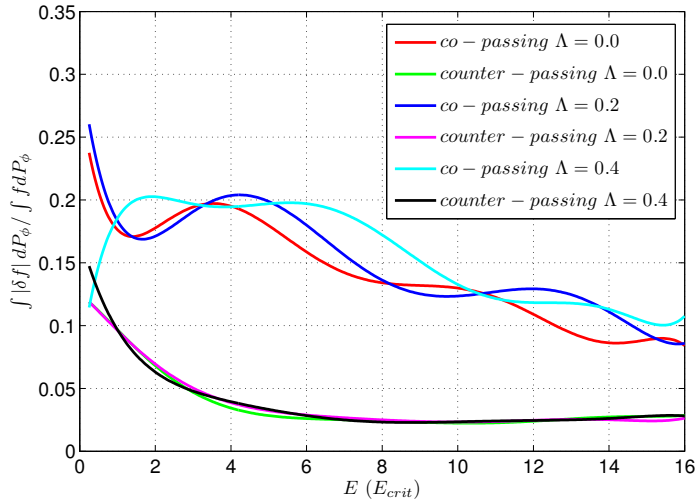


Figure 16: Redistribution level of co-passing and counter-passing particles with $\Lambda = 0.0, 0.2, 0.4$.

4 DISCUSSION AND CONCLUSION

In conclusion, we have carried out nonlinear simulations of sawteeth and energetic particle redistribution due to a sawtooth in tokamaks. In MHD simulations, we have showed repeated sawtooth oscillations similar to the Kadomtsev model for a model tokamak equilibrium. Furthermore, the M3D-K code is used to investigate energetic particle transport due to a sawtooth. The results show that energetic particles are mainly redistributed radially in central plasma region, and the distribution is reduced inside the $q = 1$ surface, and increased from the $q = 1$ surface to the sawtooth boundary, and is almost unchanged outside the sawtooth range, so energetic particles inside the $q = 1$ surface is transported out of the $q = 1$ surface due to magnetic reconnection effect, and the radial range of the redistribution is inside the sawtooth region.

In addition, the redistribution level depends on particle pitch angle and energy. For the trapped particles, there exists a critical energy above which particles are weakly redistributed, and the critical energy is approximately inversely proportional to crash time and independent of particle mass. These results are consistent with existing theories. For the passing particles, previous work showed that passing particles are strongly redistributed inside the sawtooth region. In our simulation, strong redistribution of the co-passing particles is consistent with previous prediction. In contrast, the redistribution level of the counter-passing particles has a much stronger energy dependence. The redistribution level decreases as particle energy increases. The difference between redistribution behavior of the co-passing and counter-passing particles is due to the difference in their precession frequencies. The precession frequency of the counter-passing particles is much larger than that of the co-passing particles leading to a stronger energy dependence of the counter-passing particle transport.

ACKNOWLEDGEMENTS

One of authors(Wei Shen) gratefully thanks Profs. Liu Chen and Zhiwei Ma for valuable comments. He also thanks Huishan Cai, Deyong Liu, Zhiyong Qiu, Jia Zhu, Sheng Wang, and Zhichen Feng for helpful discussions. This work was supported by the NSF of China under Grants Nos. 11075140, the ITER CN under Grant Nos. 2013GB104004 and 2009GB105005, and Fundamental Research Fund for Chinese Central Universities. The simulations were carried out using the supercomputers Hopper and Edison at NERSC.

References

- [1] S. von Goeler, W. Stodiek, and N. Sauthoff, *Phys. Rev. Lett.* **33**, 1201 (1974).
- [2] K. Ikeda, “Progress in the ITER physics basis,” *Nucl. Fusion* **47**, s128 (2007).
- [3] F. B. Marcus, J. M. Adams, A. D. Cheetham et al., *Plasma Phys. Controlled Fusion* **33**, 277 (1991).
- [4] B. C. Stratton, R.J. Ponck, G.R. McKee, R.V. Budny, Z. Chang, F. Wising, and A. Blom, *Nucl. Fusion* **36**, 1586 (1996).
- [5] S. K. Nielsen, H. Bindslev, M. Salewski et al., *Plasma Phys. Control. Fusion* **52**, 092001 (2010).
- [6] C. M. Muscatello, W. W. Heidbrink, Ya. I. Kolesnichenko, V. V. Lutsenko, M. A. Van Zeeland, and Yu. V. Yakovenko, *Plasma Phys. Control. Fusion* **54**, 025006 (2012).
- [7] S. K. Nielsen, M. Salewski, H. Bindslev et al *Nucl. Fusion* **51**, 063014 (2011).
- [8] C. M. Muscatello, B. A. Grierson, R. W. Harvey, W. W. Heidbrink, D. C. Pace, and M. A. Van Zeeland, *Nucl. Fusion* **52**, 103022 (2012).
- [9] Ya. I. Kolesnichenko and Yu. V. Yakovenko, *Nucl. Fusion* **32**, 449 (1992).
- [10] D. Anderson, Ya. I. Kolesnichenko, M. Lisak, F. Wising, and Yu. V. Yakovenko, *Nucl. Fusion* **34**, 217 (1994).
- [11] Ya. I. Kolesnichenko, and Yu. V. Yakovenko, *Nucl. Fusion* **36**, 159 (1996).
- [12] Ya. I. Kolesnichenko, V. V. Lutsenko, Yu. V. Yakovenko, and G. Kamelander, *Phys. Plasmas* **4**, 2544 (1997).
- [13] N.N. Gorelenkov, R.V. Budny, H.H. Duong, R.K. Fisher, S.S. Medley, M.P. Petrov and M.H. Redi, *Nucl. Fusion* **37**, 1053 (1997).
- [14] Ya. I. Kolesnichenko, V. V. Lutsenko, R. B. White, and Yu. V. Yakovenko, *Phys. Plasmas* **5**, 2963 (1998).
- [15] Ya. I. Kolesnichenko, V. V. Lutsenko, and Yu. V. Yakovenko, *Phys. Plasmas* **5**, 729 (1998).

- [16] Ya. I. Kolesnichenko, V. V. Lutsenko, R. B. White, Yu. V. Yakovenko, Nucl. Fusion 40, 1325 (2000).
- [17] Ya. I. Kolesnichenko, V. V. Lutsenko, R. B. White, Yu. V. Yakovenko, Phys. Lett. A 287, 131 (2001).
- [18] B. B. Kadomtsev, Sov. J. Plasma Phys. 1, 389 (1976).
- [19] Yi Zhao and Roscoe B. White, Phys. Plasmas 4, 1103 (1997).
- [20] R. Farengo, H. E. Ferrari, M.-C. Firpo, P. L. García-Martínez and A. F. Lifschitz, Plasma Phys. Control. Fusion 54, 025007 (2012).
- [21] R. Farengo, H.E. Ferrari, P.L. García-Martínez, M.-C. Firpo, W. Ettoumi and A.F. Lifschitz, Nucl. Fusion 53, 043012 (2013).
- [22] W. Park, E. V. Belova, G. Y. Fu, X. Z. Tang, H. R. Strauss, L. E. Sugiyama: Physics of Plasmas 6, 1796 (1999).
- [23] G. Y. Fu and W. Park, Phys. Rev. Lett. 74, 1594 (1995).
- [24] G. Y. Fu, W. Park, H. R. Strauss, J. Breslau, J. Chen, S. Jardin, and L. E. Sugiyama, Phys. Plasmas 13, 052517 (2006).
- [25] J. A. Breslau, S. C. Jardin, and W. Park, Phys. Plasmas 14, 056105 (2007).
- [26] J. Lang, G. Y. Fu, and Y. Chen, Phys. Plasmas 17, 042309 (2010).
- [27] H. Cai and G.Y. Fu, Phys. Plasmas 19, 072506 (2012).
- [28] F. Wang, G. Y. Fu, J. A. Breslau, K. Tritz, and J. Y. Liu, Phys. Plasmas 20, 072506 (2013).
- [29] F. Wang, G. Y. Fu, J. A. Breslau and J. Y. Liu, Phys. Plasmas 20, 102506 (2013).
- [30] R. J. Hastie, T. C. Hender, B. A. Carreras, L. A. Charlton, and J. A. Holmes, Phys. Fluids 30, 1756 (1987).
- [31] Ya. I. Kolesnichenko, R. B. White, and Yu. V. Yakovenko, Phys. Plasmas 10, 1449 (2003).
- [32] J. P. Graves, Plasma Phys. Control. Fusion 55, 074009 (2013).